

# Blind Recovery of Spatially Varying Reflectance from a Single Image

## Supplemental file

Kevin Karsch      David Forsyth  
 University of Illinois

In this document, we provide implementation details about our regression technique and initialization method, as well as additional figures to gauge our method's applicability and performance.

### Appendix A: Bias Estimation Implementation

We develop a simple regression method which does a decent job of removing bias, and produces even better results. We search for a linear prediction function  $P \in \mathbb{R}^{2 \times m}$  which maps a feature vector  $F \in \mathbb{R}^m$  to unbiased reflectance parameters.

Features are computed using histograms of gradient images and raw pixels values. Writing  $hist$  as a  $k$ -bin (we use  $k = 10$ ) normalized histogram function, we create the following feature-extracting function:

$$\mathcal{H}(I) = [hist(I), hist(\nabla_x I), hist(\nabla_y I)], \quad (1)$$

where  $\nabla_x$  and  $\nabla_y$  are horizontal and vertical gradients (in the spatial image domain) respectively.

Defining  $I$  as the input image,  $\mathbf{M}$ ,  $\mathbf{N}$ ,  $\mathbf{L}$ , as our optimized estimates ( $\mathbf{M} = (R_d^{(r)}, R_d^{(g)}, R_d^{(b)}, R_s, r)$  is material,  $\mathbf{N}$  is per-pixel surface normals, and  $\mathbf{L}$  is the lighting parameters). Furthermore, let  $R = f(\mathbf{M}, \mathbf{N}, \mathbf{L})$  be the final reconstructed (rendered) image from these optimized estimates. We compute a feature vector as:

$$F = [1, R_s, r, \mathcal{H}(I), \mathcal{H}(R), \mathcal{H}(\|I - R\|^2), \mathcal{H}(\mathbf{N})] \quad (2)$$

Given a set of results from our optimization technique with ground truth material parameters  $b = [R_s^{true}, r^{true}]$ , we solve for  $P$  by minimizing an L<sub>1</sub> regression problem (with L<sub>2</sub> regularization):

$$\underset{P}{\text{minimize}} \left| P[F_1^T, \dots, F_n^T] - [b_1^T, \dots, b_n^T] \right| + w\|P\|^2 \quad (3)$$

where  $F_i$  and  $b_i$  are the feature vector and true material for the  $i^{th}$  training example, and  $w = 0.1$  is the regularization coefficient.

### Appendix B: Initialization Details

Our goal is to simultaneously adjust estimates of reflectance, shape and illumination to match an image, and this results in a non-convex optimization problem with many local minima; thus, our initial estimates are crucial. We propose an intuitive solution that works well in practice, although other methods may suffice or even perform better. First, shape is initialized using a simple shape-from-contour method: boundary normals are perpendicular to the viewing direction and contour, and smoothed inwards, resulting in a “blobby” convex object. Next, we initialize illumination by hough voting;

each pixel in the input image votes (weighted by pixel intensity) for a light direction. The hough map is smoothed to prune spurious peaks, and then we initialize Gaussians centered at each of the remaining peaks. The other illumination parameters (spherical harmonic coefficients, Gaussian concentration, etc) are initialized using the means (per-parameter) from our fitting results on our illumination dataset (see the main paper for details). We use initial shape and illumination to initialize diffuse reflectance by computing per-pixel irradiance, and then averaging over quotient of the image and irradiance. Specular parameters are initialized to be low (0.01 for each), which results in a somewhat glossy appearance. Fig 4 demonstrates this procedure for two images in our dataset.

### List of additional figures

- Fig 1: Example failure cases
- Fig 2: Illumination used to compute cross render error
- Fig 3: Parameter fitting results on our illumination dataset
- Fig 4: Examples of our initialization procedure
- Fig 5: Comparison of our hybrid light model with SH
- Fig 6: Results for different initializations
- Fig 7–16: Comprehensive optimization/regression results.  
 We show material  $i$  and shape  $i$  from our dataset  
 $(i = \{2, 4, \dots, 20\})$ ; i.e. these are not chosen by error/etc.
- Fig 17: Material editing using our method
- Fig 18: Effects of different firmness parameter settings
- Fig 19: Material transfer for wood

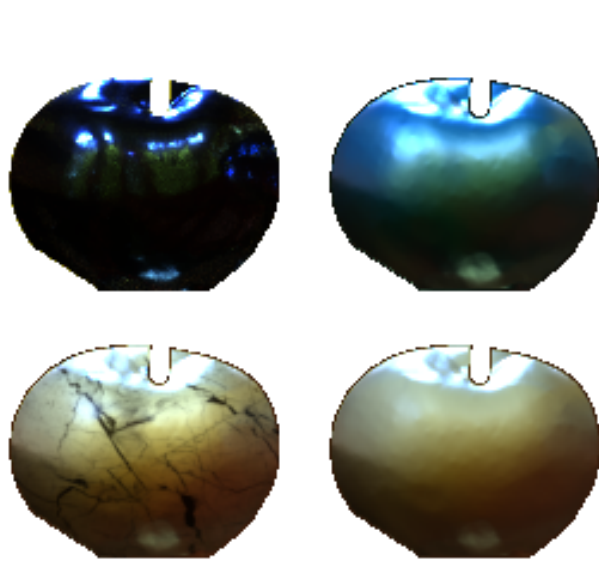


**Figure 1:** Typical failure examples caused by complex BRDFs (top) and spatially varying materials (bottom). On the left are two input images, and on the right are our results (estimated material rendered on true shape in true light). Our model is not well suited to fit certain complex reflectance functions (anisotropic BRDFs, chromatic specular lobes, etc), and our model cannot handle spatial variation in material; these are directions for future work.



**Figure 2:** The six illumination environments (tonemapped for visualization) used when computing our cross render error metric. These six environments are not used in our 400-image material datasets, and are representative of many common, real-world environments (indoors, outdoor, natural light, man-made light, etc). To compute cross-render error for a given material estimate, we render an object with the true material and our estimated material in each of these lighting environments, and compute the average  $L_2$  pixel error for each pair of rendered images.

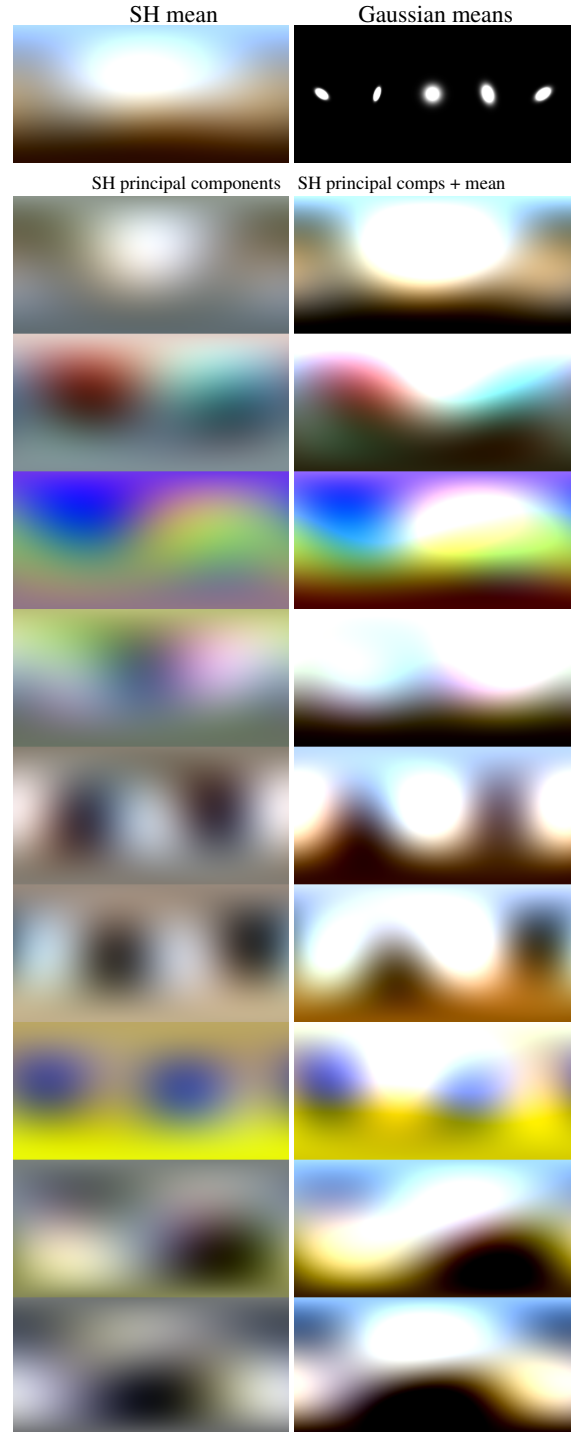


**Figure 3:** Parameter fitting and analysis on our illumination dataset. First, we fit our lighting model to each of our 200 spherical illumination images (IBLs). For spherical harmonics, we extract the mean (top left) and principal component vectors for each channel (bottom left; normalized to  $[0,1]$  and sorted by decreasing eigenvalue). The bottom right shows the mean spherical harmonics added to each eigenvector. We cluster Gaussian concentration and ellipticalness parameters (from our illumination fitting) into 5 clusters, and display  $i = \{1, \dots, 5\}$  Gaussians using the  $i^{\text{th}}$  concentration mean and  $i^{\text{th}}$  ellipticalness mean (top right).

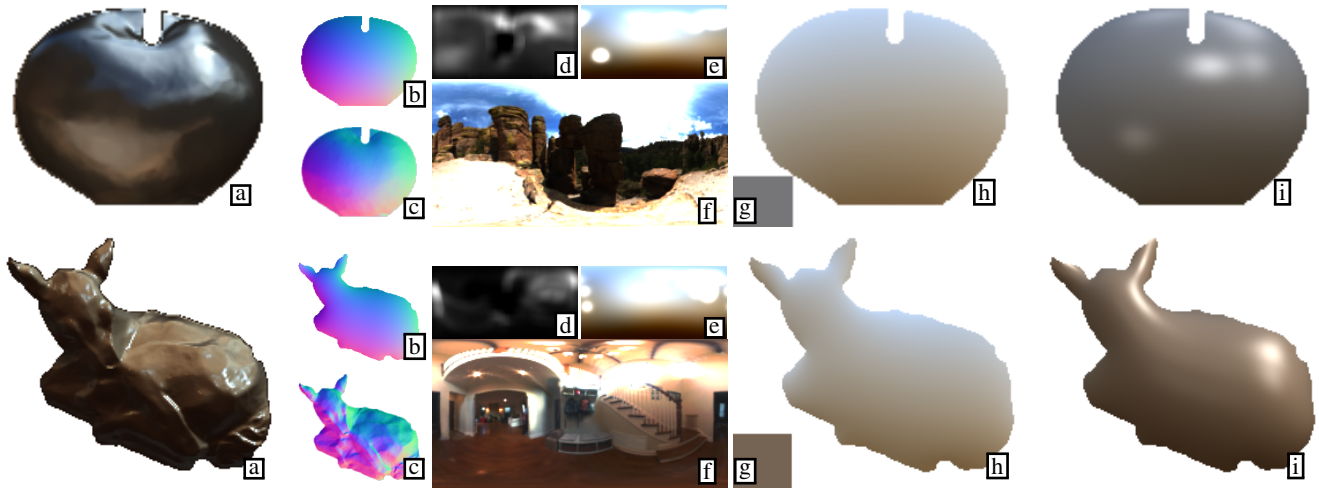


**Figure 4:** Two examples of our initialization procedure. We start with a masked input image (a), and use shape-from-contour to estimate initial shape (b); ground truth shape displayed below (c). Using the input image and initial shape, we compute a hough map of potential light source directions (d), and initialize illumination using the hough map as well as parameters fit from a dataset of real illumination environments (e); ground truth light displayed below (f). We estimate initial diffuse albedo (g) by computing irradiance using our initial shape and light (h), dividing irradiance by the input (per-pixel), and averaging across each channel. Specular parameters are initialized as constants. A rendering produced by our initial shape, light, and material is shown in (i).

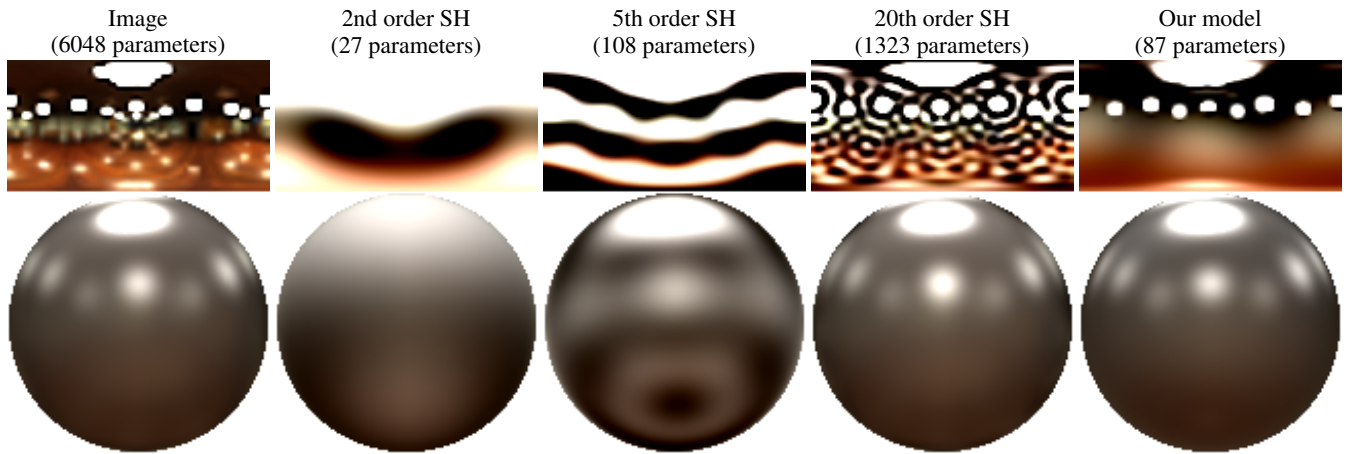


**Figure 5:** Illumination environment fit using different lighting models (top) and the renderings they produce (bottom). Parameterizing illumination with a grid of image pixels produces good renderings but uses far too many parameters (left). An alternative is using spherical harmonics (middle columns) which works well for diffuse materials, but requires numerous parameters to handle most specular materials due to difficulty in localizing high frequencies (Gibbs phenomenon). Our hybrid model (SH+Gaussian mixture) is low-order and still produces realistic renderings. We typically achieve results comparable to 20th order spherical harmonic fits, but with about as many parameters as 5th order SH.

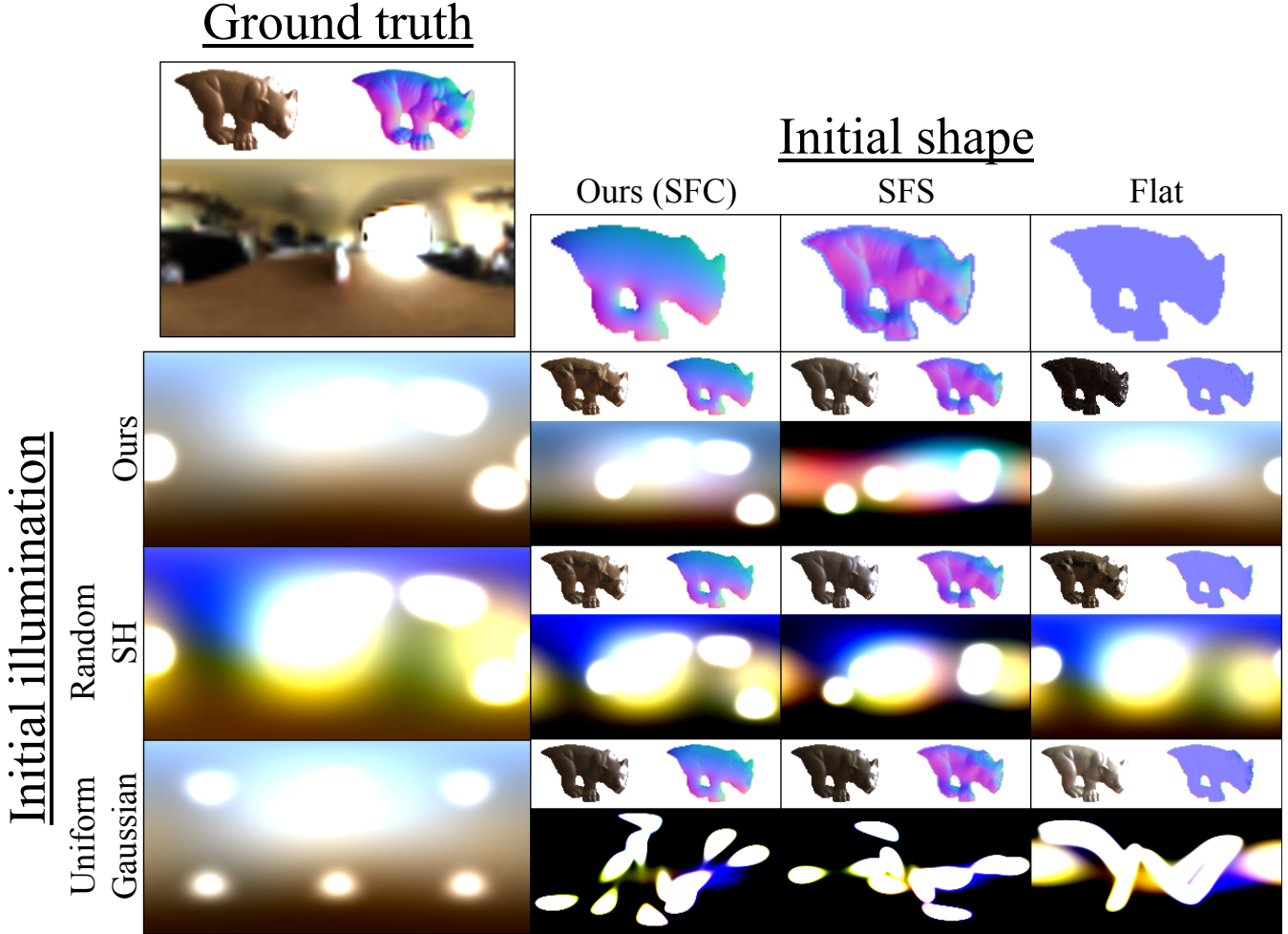


**Figure 6:** Optimization results using different initialization methods for shape and illumination. For shape, we initialize using our method (shape-from-contour), a shape-from-shading method (per Barron and Malik), and with a flat shape (all normals point at the camera). Illumination is initialized as: Ours – our method (see Appendix B and Fig 4); Random SH – we use our initial lighting, but perturb the spherical harmonic coefficients randomly; Uniform Gaussian – our initial lighting, but the Gaussian centers are redistributed uniformly over the sphere. Each block within the  $3 \times 3$  grid corresponds to a given shape/lighting initialization, and shows the resulting material (rendered on true shape and in true light), as well as the final estimate of shape and illumination. As expected, we observe that our method is sensitive to the starting point, but seems tolerant of the choice of spherical harmonic initialization. This is likely because the Gaussian components usually dominate rendered appearance since they try to encode direct lighting, whereas SH coefficients attempt to encode indirect lighting; this is also perhaps why a poor Gaussian initialization leads to degraded results. It is interesting to see that some resulting materials look very similar (and close to ground truth), yet the estimated shape and illumination appears much different; we believe this is due to our rigid, 5-parameter material model.

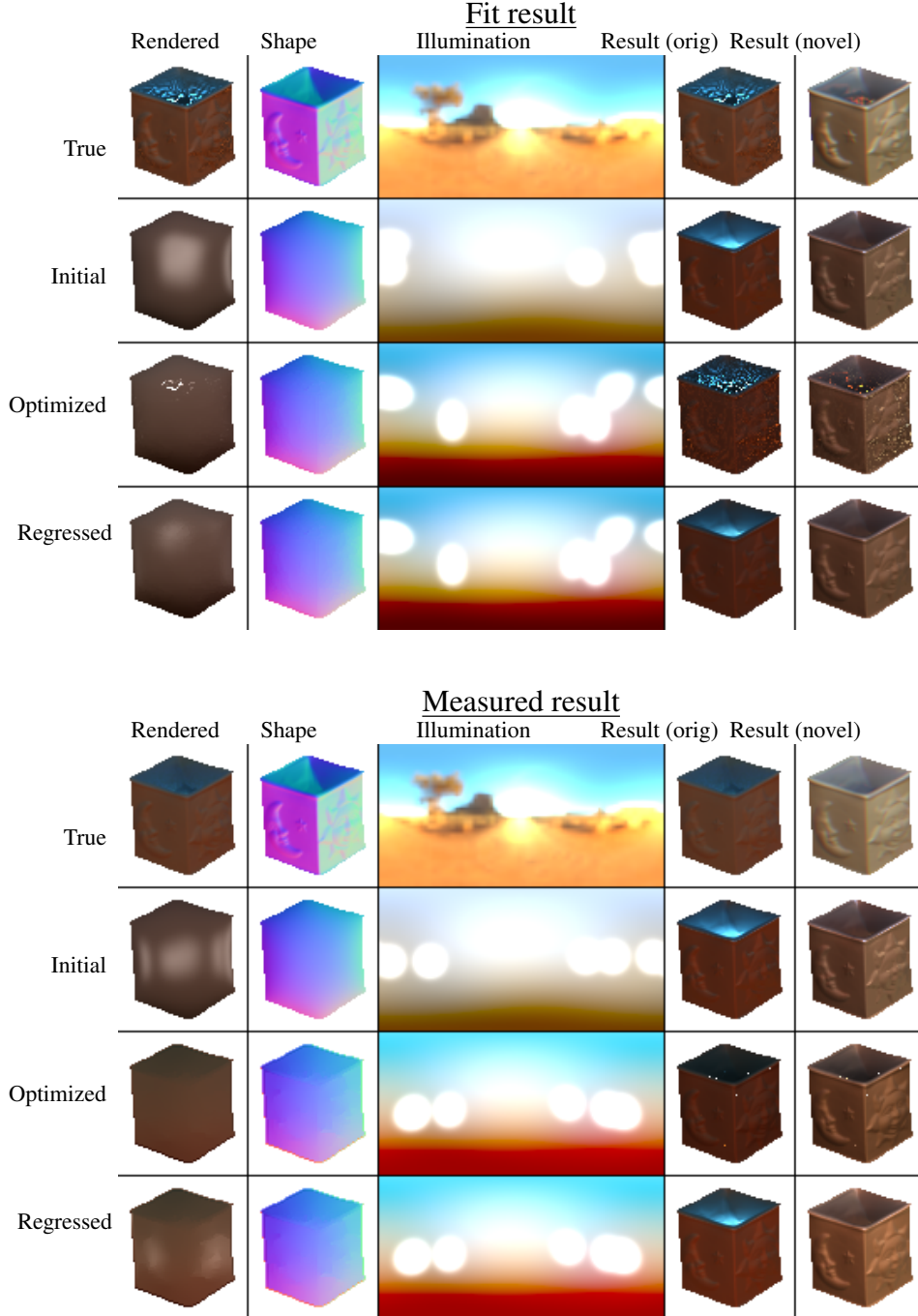


**Figure 7:** Optimization and regression results for both “fit” and “measured” datasets. By column: rendered – a rendering of the estimate shape, light, and material; shape – estimated surface normals (normalized for display); illumination – spherical illumination mapped to the latitude/longitude domain; results – rendering of estimated material onto true shape in true illumination; orig implies rendered into the original illumination, novel implies rendering into novel illumination (e.g. bottom left of Fig 2). By row: true values; our initialized estimates (per Fig 4); estimates after running our optimization; estimates after hold-one-out regression. We observe that our estimates tend towards the correct parameters, but degrade for complex materials (e.g. some of those in the measured dataset). Despite this, our estimates still achieve low error (beating reasonable baselines) on both datasets, and our optimization and regression techniques clearly improve upon initial estimates. Most importantly, we are the first to extract specular material parameters from a single image without any knowledge of shape or illumination.

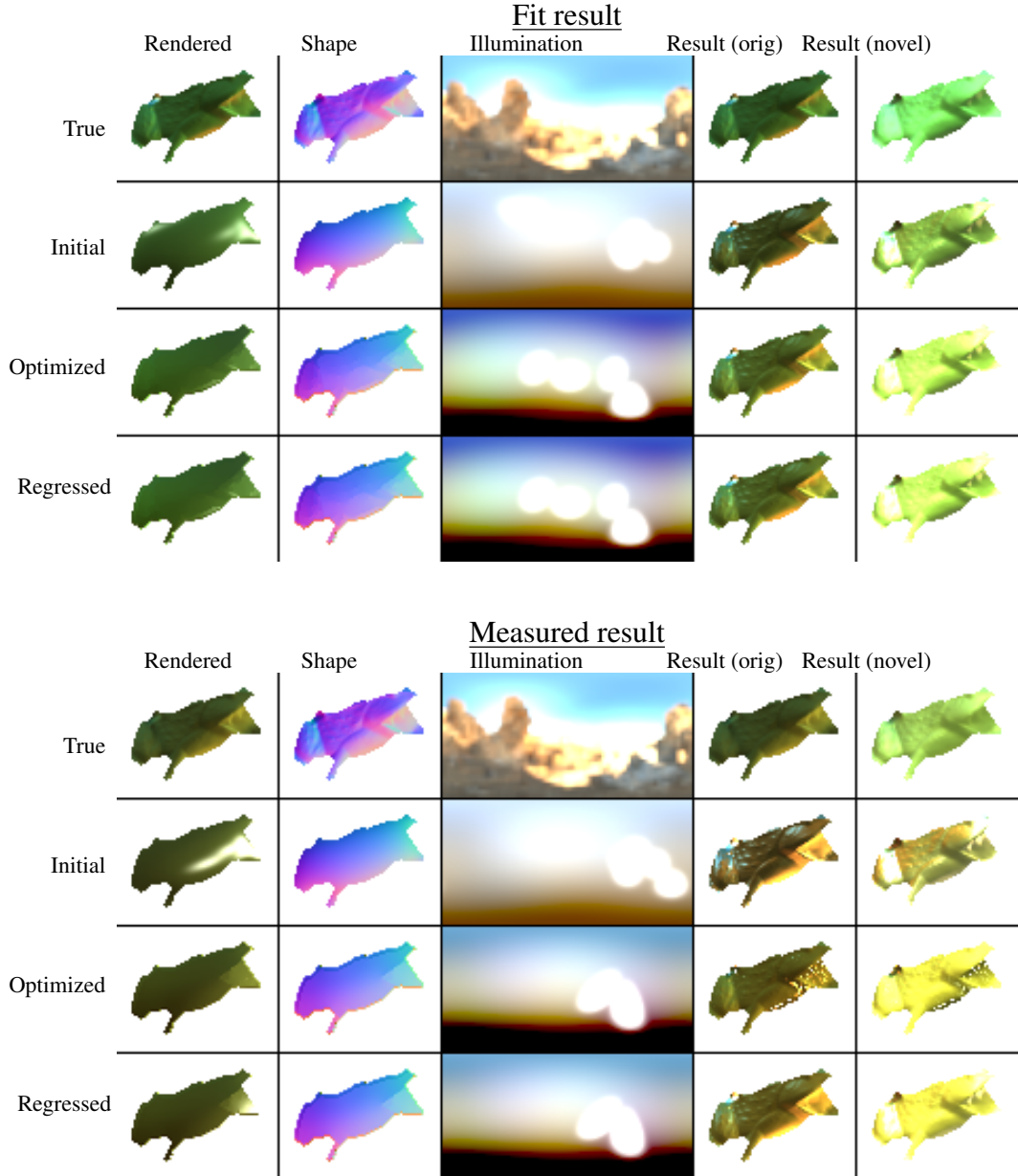


**Figure 8:** Optimization and regression results for both “fit” and “measured” datasets. By column: rendered – a rendering of the estimate shape, light, and material; shape – estimated surface normals (normalized for display); illumination – spherical illumination mapped to the latitude/longitude domain; results – rendering of estimated material onto true shape in true illumination; orig implies rendered into the original illumination, novel implies rendering into novel illumination (e.g. bottom left of Fig 2). By row: true values; our initialized estimates (per Fig 4); estimates after running our optimization; estimates after hold-one-out regression. We observe that our estimates tend towards the correct parameters, but degrade for complex materials (e.g. some of those in the measured dataset). Despite this, our estimates still achieve low error (beating reasonable baselines) on both datasets, and our optimization and regression techniques clearly improve upon initial estimates. Most importantly, we are the first to extract specular material parameters from a single image without any knowledge of shape or illumination.

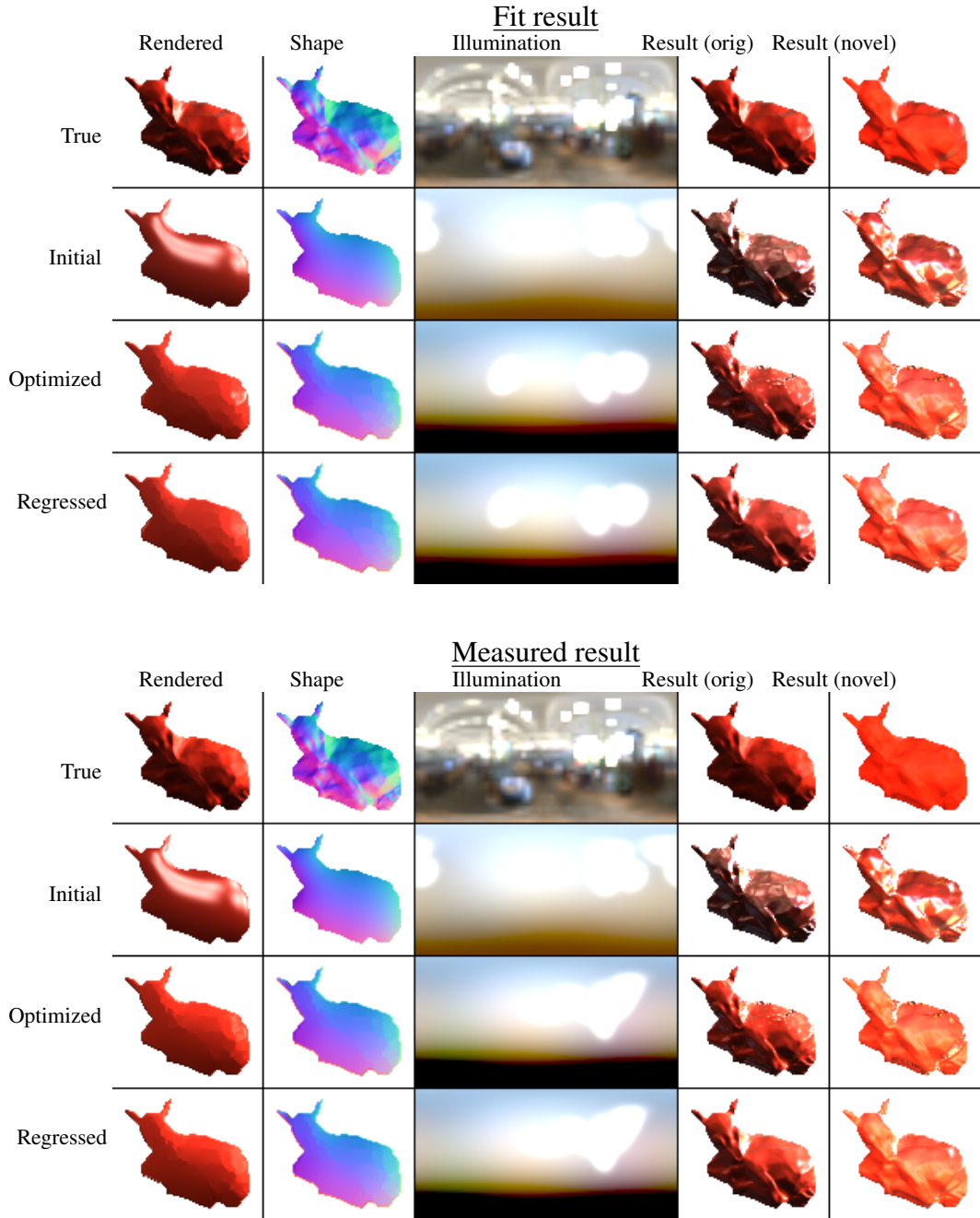


**Figure 9:** Optimization and regression results for both “fit” and “measured” datasets. By column: rendered – a rendering of the estimate shape, light, and material; shape – estimated surface normals (normalized for display); illumination – spherical illumination mapped to the latitude/longitude domain; results – rendering of estimated material onto true shape in true illumination; orig implies rendered into the original illumination, novel implies rendering into novel illumination (e.g. bottom left of Fig 2). By row: true values; our initialized estimates (per Fig 4); estimates after running our optimization; estimates after hold-one-out regression. We observe that our estimates tend towards the correct parameters, but degrade for complex materials (e.g. some of those in the measured dataset). Despite this, our estimates still achieve low error (beating reasonable baselines) on both datasets, and our optimization and regression techniques clearly improve upon initial estimates. Most importantly, we are the first to extract specular material parameters from a single image without any knowledge of shape or illumination.

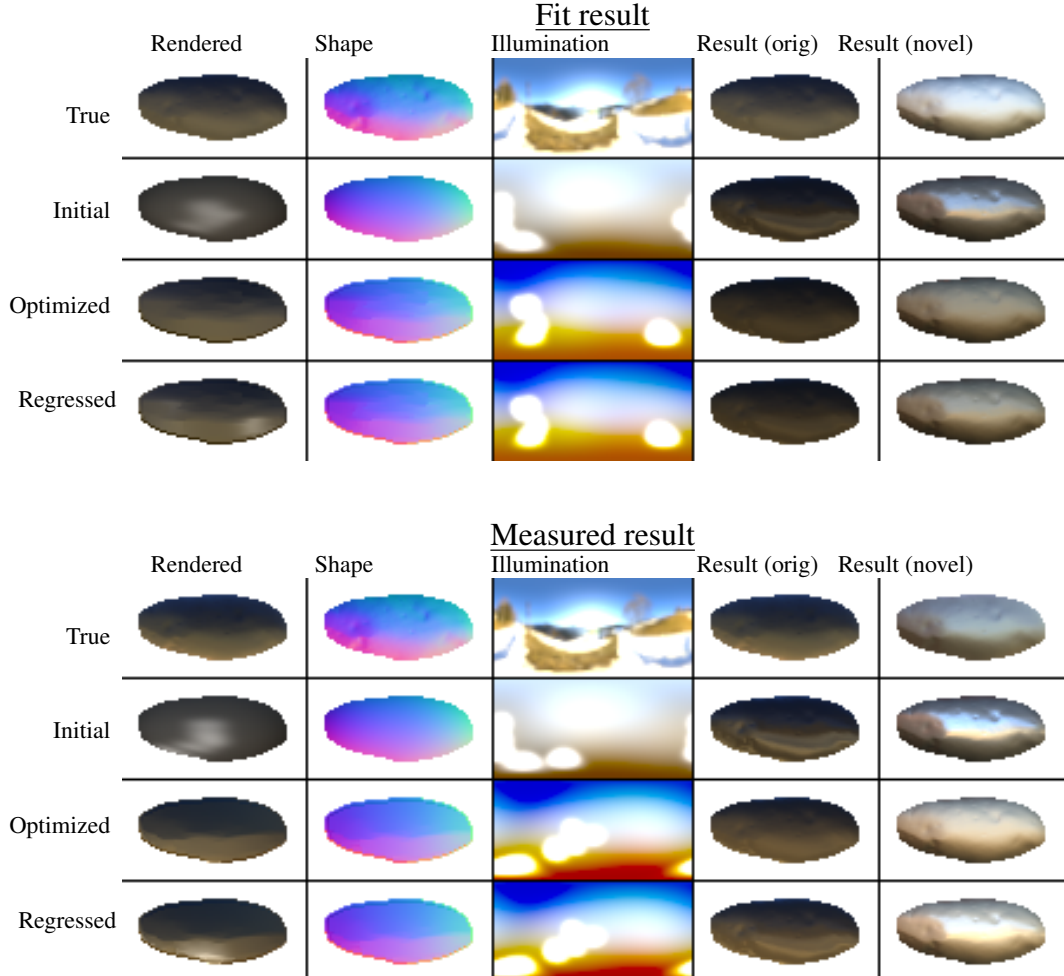


**Figure 10:** Optimization and regression results for both “fit” and “measured” datasets. By column: rendered – a rendering of the estimate shape, light, and material; shape – estimated surface normals (normalized for display); illumination – spherical illumination mapped to the latitude/longitude domain; results – rendering of estimated material onto true shape in true illumination; orig implies rendered into the original illumination, novel implies rendering into novel illumination (e.g. bottom left of Fig 2). By row: true values; our initialized estimates (per Fig 4); estimates after running our optimization; estimates after hold-one-out regression. We observe that our estimates tend towards the correct parameters, but degrade for complex materials (e.g. some of those in the measured dataset). Despite this, our estimates still achieve low error (beating reasonable baselines) on both datasets, and our optimization and regression techniques clearly improve upon initial estimates. Most importantly, we are the first to extract specular material parameters from a single image without any knowledge of shape or illumination.

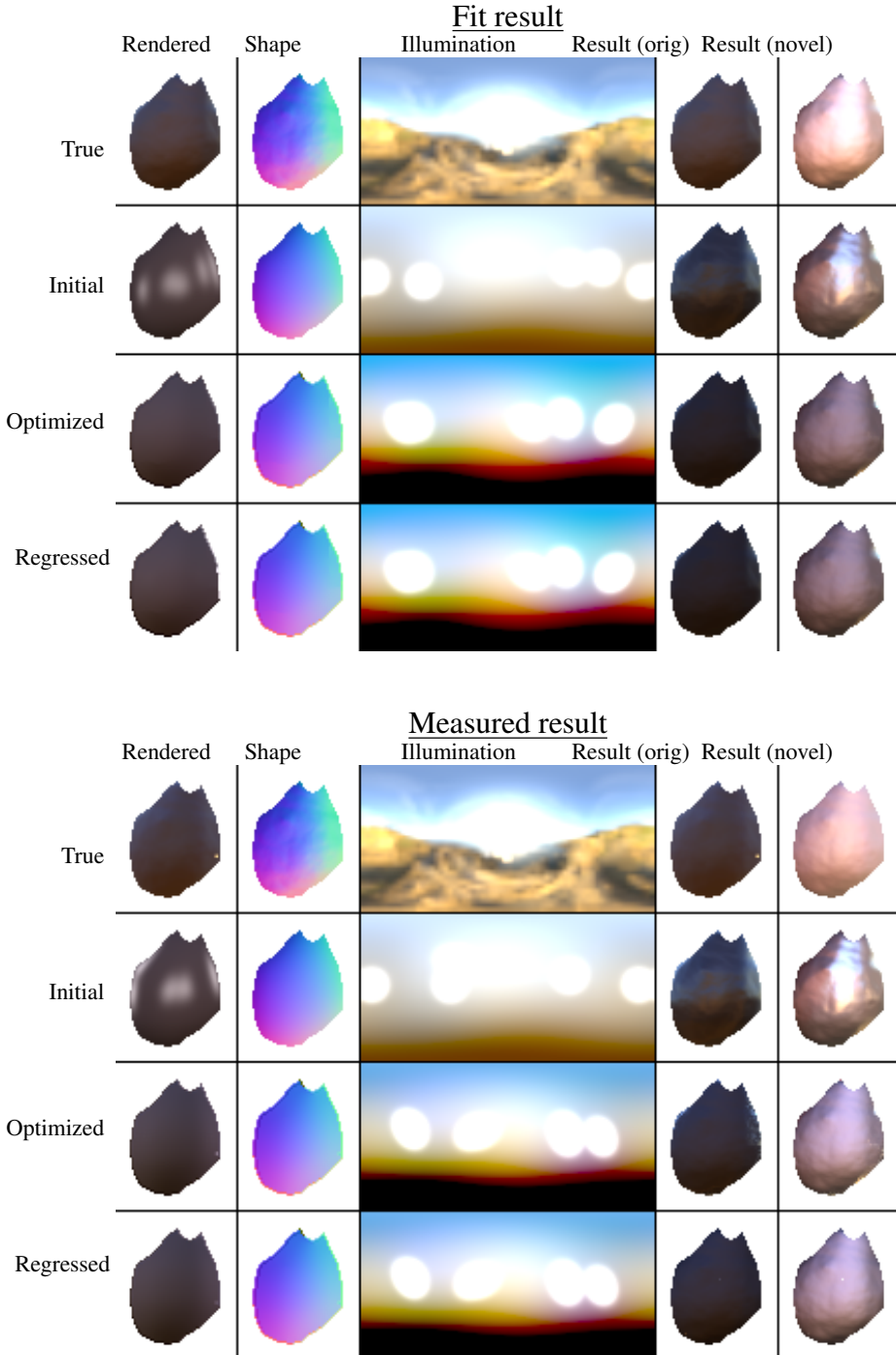


**Figure 11:** Optimization and regression results for both “fit” and “measured” datasets. By column: rendered – a rendering of the estimate shape, light, and material; shape – estimated surface normals (normalized for display); illumination – spherical illumination mapped to the latitude/longitude domain; results – rendering of estimated material onto true shape in true illumination; orig implies rendered into the original illumination, novel implies rendering into novel illumination (e.g. bottom left of Fig 2). By row: true values; our initialized estimates (per Fig 4); estimates after running our optimization; estimates after hold-one-out regression. We observe that our estimates tend towards the correct parameters, but degrade for complex materials (e.g. some of those in the measured dataset). Despite this, our estimates still achieve low error (beating reasonable baselines) on both datasets, and our optimization and regression techniques clearly improve upon initial estimates. Most importantly, we are the first to extract specular material parameters from a single image without any knowledge of shape or illumination.

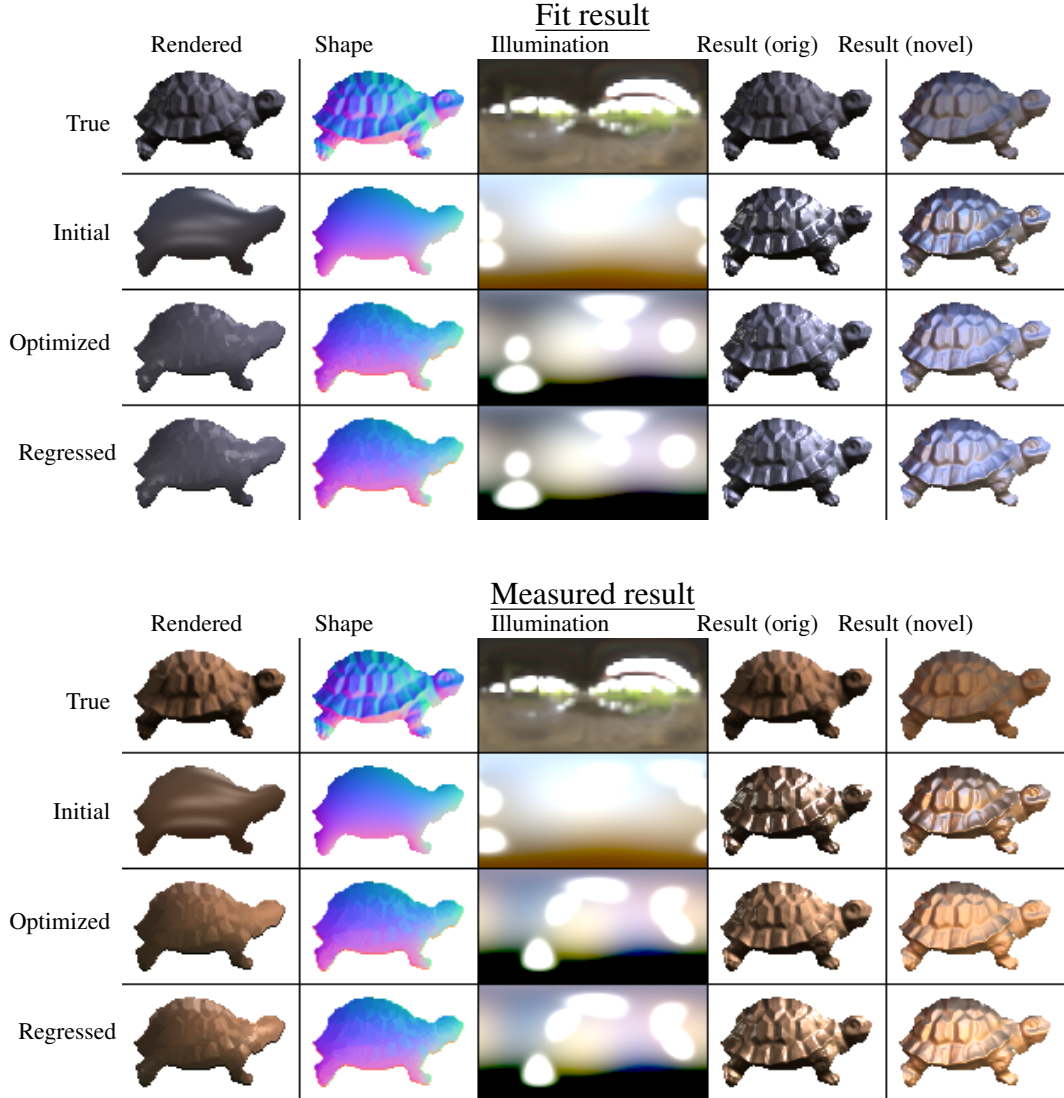


**Figure 12:** Optimization and regression results for both “fit” and “measured” datasets. By column: rendered – a rendering of the estimate shape, light, and material; shape – estimated surface normals (normalized for display); illumination – spherical illumination mapped to the latitude/longitude domain; results – rendering of estimated material onto true shape in true illumination; orig implies rendered into the original illumination, novel implies rendering into novel illumination (e.g. bottom left of Fig 2). By row: true values; our initialized estimates (per Fig 4); estimates after running our optimization; estimates after hold-one-out regression. We observe that our estimates tend towards the correct parameters, but degrade for complex materials (e.g. some of those in the measured dataset). Despite this, our estimates still achieve low error (beating reasonable baselines) on both datasets, and our optimization and regression techniques clearly improve upon initial estimates. Most importantly, we are the first to extract specular material parameters from a single image without any knowledge of shape or illumination.

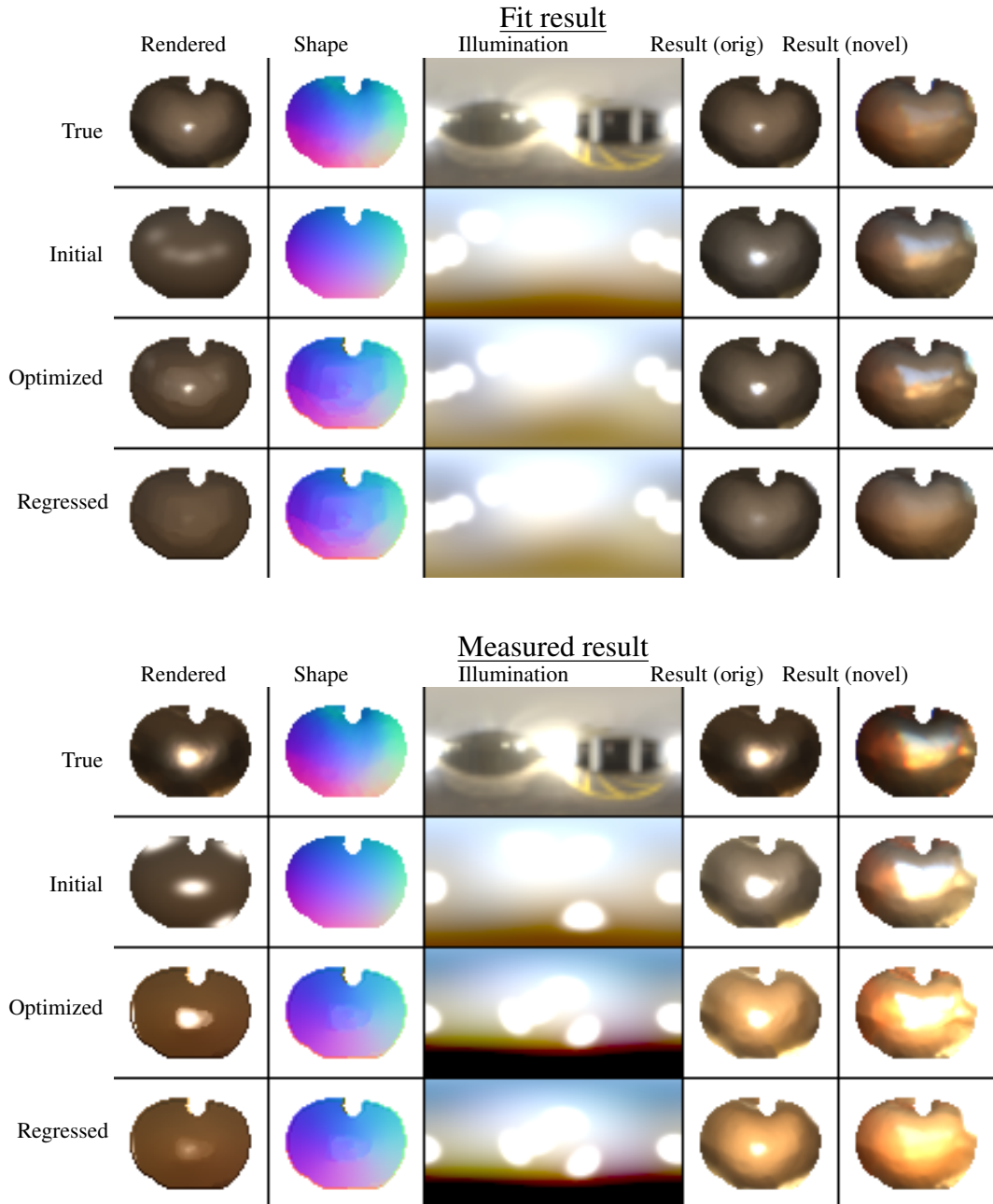


**Figure 13:** Optimization and regression results for both “fit” and “measured” datasets. By column: rendered – a rendering of the estimate shape, light, and material; shape – estimated surface normals (normalized for display); illumination – spherical illumination mapped to the latitude/longitude domain; results – rendering of estimated material onto true shape in true illumination; orig implies rendered into the original illumination, novel implies rendering into novel illumination (e.g. bottom left of Fig 2). By row: true values; our initialized estimates (per Fig 4); estimates after running our optimization; estimates after hold-one-out regression. We observe that our estimates tend towards the correct parameters, but degrade for complex materials (e.g. some of those in the measured dataset). Despite this, our estimates still achieve low error (beating reasonable baselines) on both datasets, and our optimization and regression techniques clearly improve upon initial estimates. Most importantly, we are the first to extract specular material parameters from a single image without any knowledge of shape or illumination.

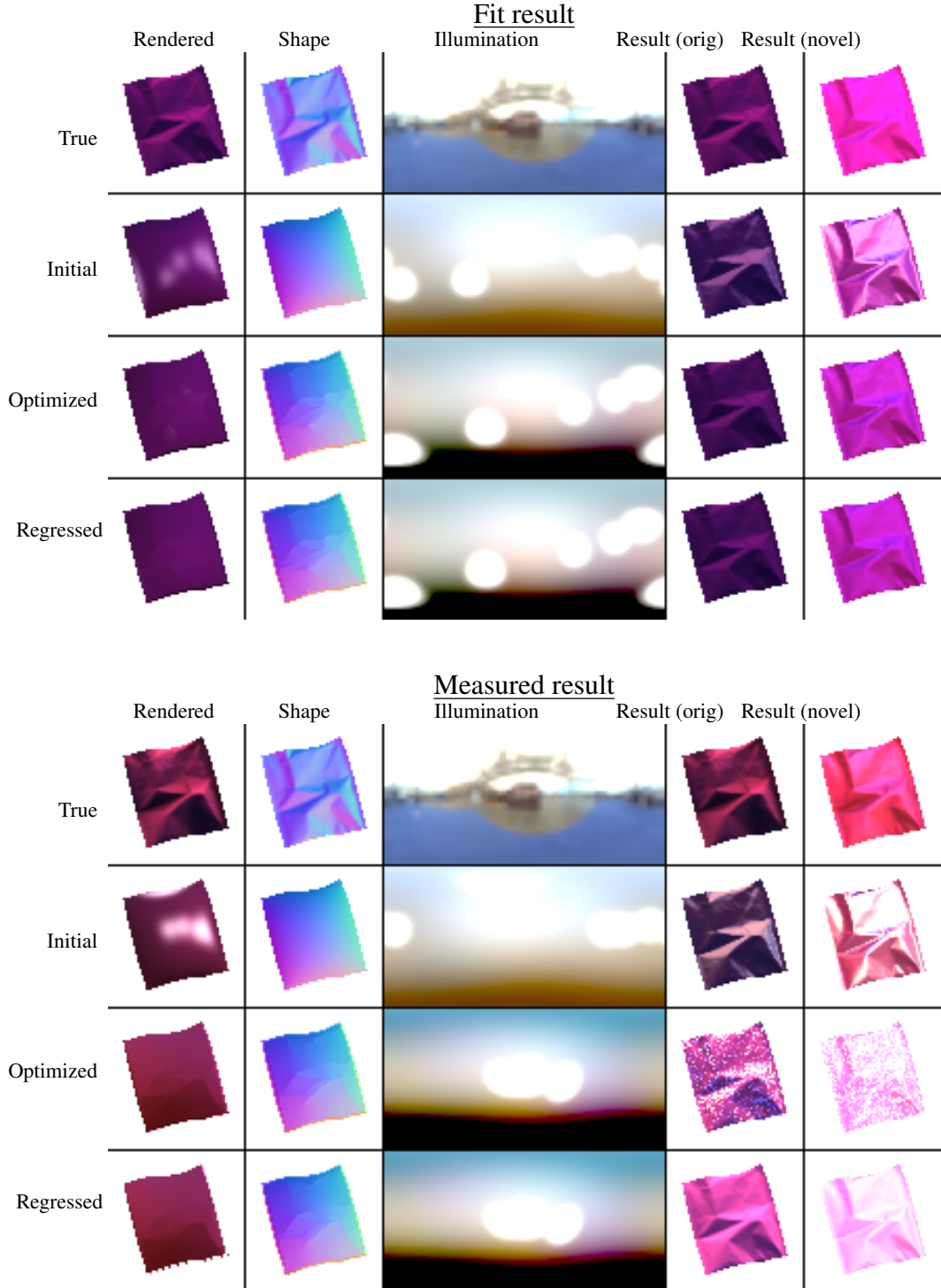


**Figure 14:** Optimization and regression results for both “fit” and “measured” datasets. By column: rendered – a rendering of the estimate shape, light, and material; shape – estimated surface normals (normalized for display); illumination – spherical illumination mapped to the latitude/longitude domain; results – rendering of estimated material onto true shape in true illumination; orig implies rendered into the original illumination, novel implies rendering into novel illumination (e.g. bottom left of Fig 2). By row: true values; our initialized estimates (per Fig 4); estimates after running our optimization; estimates after hold-one-out regression. We observe that our estimates tend towards the correct parameters, but degrade for complex materials (e.g. some of those in the measured dataset). Despite this, our estimates still achieve low error (beating reasonable baselines) on both datasets, and our optimization and regression techniques clearly improve upon initial estimates. Most importantly, we are the first to extract specular material parameters from a single image without any knowledge of shape or illumination.

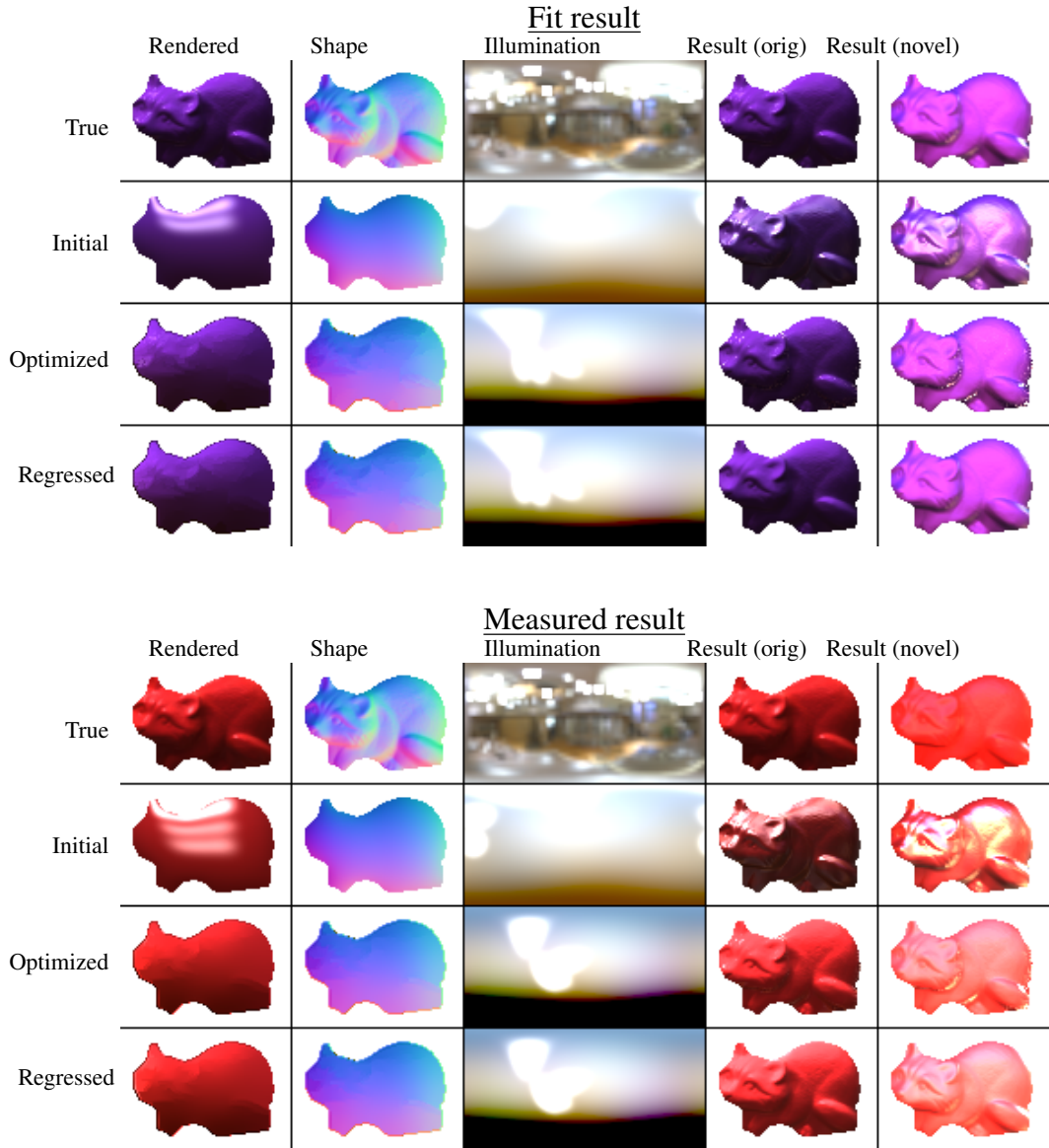


**Figure 15:** Optimization and regression results for both “fit” and “measured” datasets. By column: rendered – a rendering of the estimate shape, light, and material; shape – estimated surface normals (normalized for display); illumination – spherical illumination mapped to the latitude/longitude domain; results – rendering of estimated material onto true shape in true illumination; orig implies rendered into the original illumination, novel implies rendering into novel illumination (e.g. bottom left of Fig 2). By row: true values; our initialized estimates (per Fig 4); estimates after running our optimization; estimates after hold-one-out regression. We observe that our estimates tend towards the correct parameters, but degrade for complex materials (e.g. some of those in the measured dataset). Despite this, our estimates still achieve low error (beating reasonable baselines) on both datasets, and our optimization and regression techniques clearly improve upon initial estimates. Most importantly, we are the first to extract specular material parameters from a single image without any knowledge of shape or illumination.

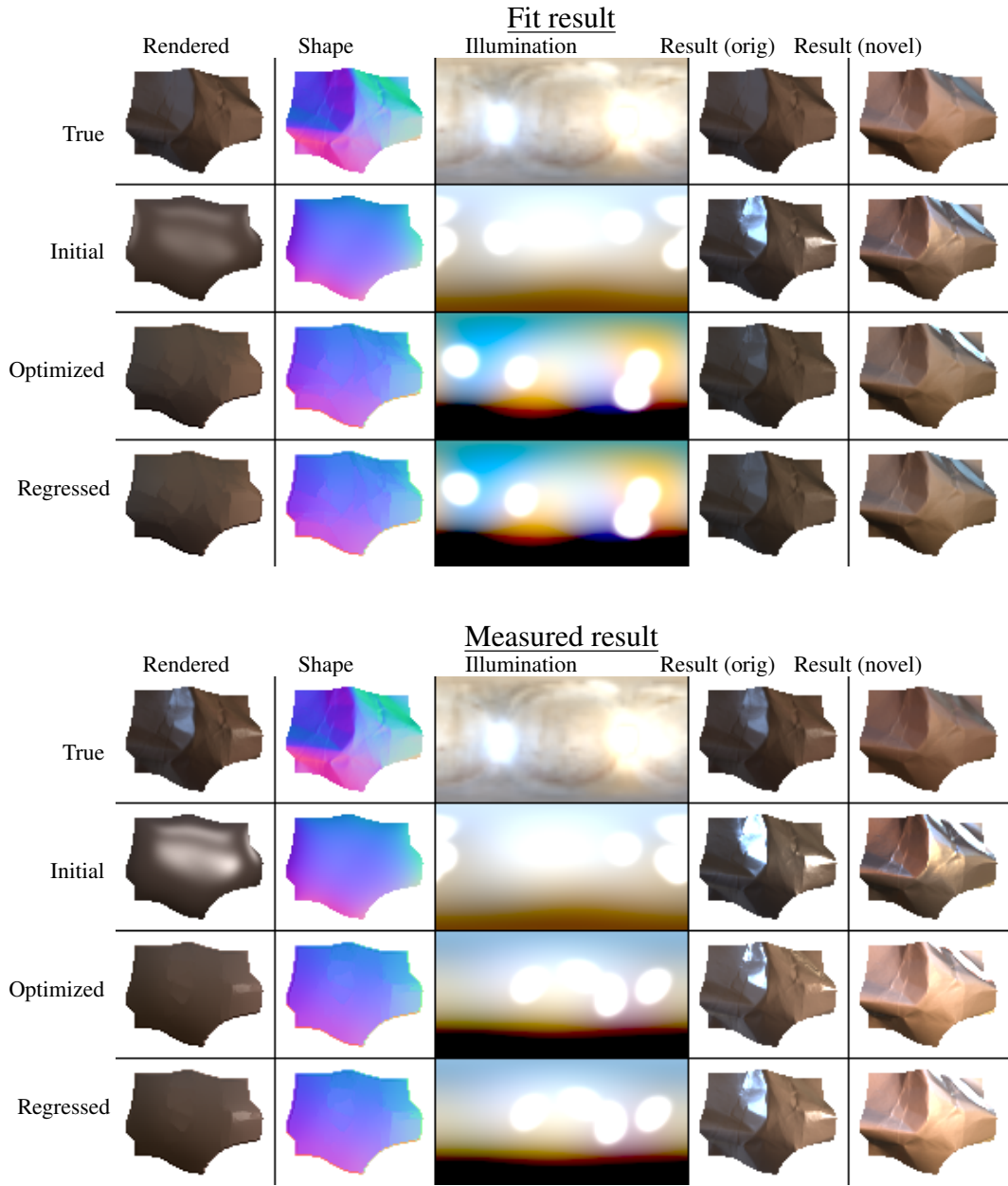


**Figure 16:** Optimization and regression results for both “fit” and “measured” datasets. By column: rendered – a rendering of the estimate shape, light, and material; shape – estimated surface normals (normalized for display); illumination – spherical illumination mapped to the latitude/longitude domain; results – rendering of estimated material onto true shape in true illumination; orig implies rendered into the original illumination, novel implies rendering into novel illumination (e.g. bottom left of Fig 2). By row: true values; our initialized estimates (per Fig 4); estimates after running our optimization; estimates after hold-one-out regression. We observe that our estimates tend towards the correct parameters, but degrade for complex materials (e.g. some of those in the measured dataset). Despite this, our estimates still achieve low error (beating reasonable baselines) on both datasets, and our optimization and regression techniques clearly improve upon initial estimates. Most importantly, we are the first to extract specular material parameters from a single image without any knowledge of shape or illumination.

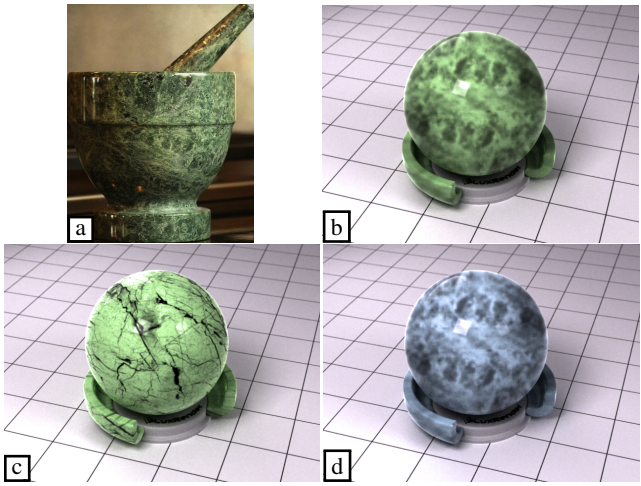


**Figure 17:** Material editing using our method. First, we transfer one material to another surface (a,b). Then, a user can optionally specify a new spatial mixture (c) or new materials (d).

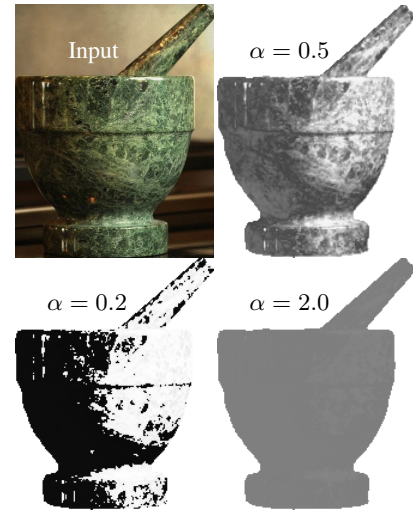


**Figure 18:** Different firmness settings ( $\alpha$ ). This parameter allows greater control over the spatial mixing structure; we use  $\alpha = 0.5$ .

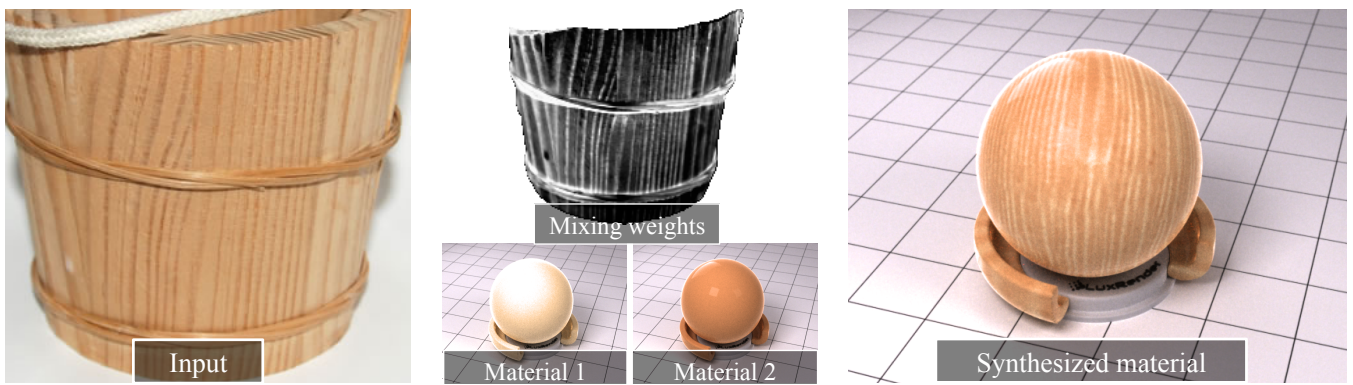


**Figure 19:** Material transfer for wood.